

The Fe XXII I(11.92 Å)/I(11.77 Å) Density Diagnostic Applied to the Chandra High Energy Transmission Grating Spectrum of EX Hydrae

Christopher W. Mauche, Duane A. Liedahl, and Kevin B. Fournier

Lawrence Livermore National Laboratory, L-473, 7000 East Avenue, Livermore, CA 94550;
mauche@cygnus.llnl.gov, liedahl1@llnl.gov, fournier2@llnl.gov

ABSTRACT

Using the Livermore X-ray Spectral Synthesizer, which calculates spectral models of highly charged ions based primarily on HULLAC atomic data, we investigate the temperature, density, and photoexcitation dependence of the $I(11.92 \text{ \AA})/I(11.77 \text{ \AA})$ line ratio of Fe XXII. We find that this line ratio has a critical density $n_c \approx 5 \times 10^{13} \text{ cm}^{-3}$, is approximately 0.3 at low densities and 1.5 at high densities, and is very insensitive to temperature and photoexcitation, so is a useful density diagnostic for sources like magnetic cataclysmic variables in which the plasma densities are high and the efficacy of the He-like ion density diagnostic is compromised by the presence of a bright ultraviolet continuum. Applying this diagnostic to the *Chandra* High Energy Transmission Grating spectrum of the intermediate polar EX Hya, we find that the electron density of its $T_e \approx 12 \text{ MK}$ plasma is $n_e = 1.0_{-0.5}^{+2.0} \times 10^{14} \text{ cm}^{-3}$, orders of magnitude greater than that typically observed in the Sun or other late-type stars.

Subject headings: atomic processes — binaries: close — stars: individual (EX Hydrae)
 — stars: magnetic fields — X-rays: binaries

1. Introduction

Magnetic cataclysmic variables (mCVs; polars and intermediate polars) are bright X-ray sources because the highly supersonic [free-fall velocity $v_{\text{ff}} = (2GM_{\text{wd}}/R_{\text{wd}})^{1/2} \approx 3600 \text{ km s}^{-1}$] material raining down on the white dwarf primary passes through a strong shock where most of its kinetic energy is converted into thermal energy and the plasma is heated to a temperature $T_s = 3GM_{\text{wd}}\mu m_{\text{H}}/8kR_{\text{wd}} \approx 200 \text{ MK}$. Because of the magnetic funneling of the mass lost by the secondary, the factor-of-four density jump across the accretion shock, and the settling nature of the post-shock flow (wherein the pressure is roughly constant and the density scales inversely with the temperature; Frank, King, & Raine 1992), the hot plasma in mCVs is expected to be dense. For a mass-accretion rate $\dot{M} = 10^{15} \text{ g s}^{-1}$ ($L_X = GM_{\text{wd}}\dot{M}/2R_{\text{wd}} \approx 3 \times 10^{31} \text{ erg s}^{-1}$) and a relative spot

size $f = 0.1$, the density of the flow immediately behind the shock is $n = \dot{M}/4\pi f R_{\text{wd}}^2 \mu m_{\text{H}} (v_{\text{ff}}/4) \approx 10^{13} \text{ cm}^{-3}$.

The standard density diagnostic of high-temperature plasmas is the intensity ratio $R \equiv f/i$ of the forbidden to intercombination lines of He-like ions (Gabriel & Jordan 1969; Blumenthal, Drake, & Tucker 1972; Porquet et al. 2001), but this diagnostic is compromised in mCVs for two reasons. First, the critical density of this ratio increases with Z and hence temperature—the opposite of the trend in the accretion column—so the R line ratio is effective over only a very narrow slice of the accretion column. Second, in mCVs and other ultraviolet-bright stars, photoexcitation competes with collisional excitation to depopulate the upper level of the forbidden line, so the R line ratio can appear to be in the “high-density limit” if the radiation field is sufficiently strong at the appropriate wavelengths: for a plasma illuminated by a 30 kK blackbody, the R line ratios of all elements through Mg lie in the high-density limit, regardless of the density (Mauche 2002).

To circumvent the density/photoexcitation ambiguity of the R line ratio of He-like ions, we undertook an investigation of potential density diagnostics of lines of Fe L-shell ions that are observable in the high quality *Chandra* High Energy Transmission Grating (HETG) spectrum of the intermediate polar EX Hya (Mauche 2000, 2002). Toward this end, Mauche, Liedahl, & Fournier (2001) investigated the density, temperature, and photoexcitation dependence of the $I(17.10 \text{ \AA})/I(17.05 \text{ \AA})$ line ratio of Fe XVII, and found that the anomalous ratio observed in EX Hya can be explained if the electron density of its $T_e \approx 4$ MK plasma is $n_e \gtrsim 2 \times 10^{14} \text{ cm}^{-3}$ or if the photoexcitation temperature $T_{\text{bb}} \gtrsim 55$ kK. In this *Letter*, we investigate the density, temperature, and photoexcitation dependence of the $I(11.92 \text{ \AA})/I(11.77 \text{ \AA})$ line ratio of Fe XXII, which also is anomalous in EX Hya. We find that this line ratio is very insensitive to temperature and photoexcitation and that the observed ratio can be explained if the electron density of EX Hya’s $T_e \approx 12$ MK plasma is $n_e \approx 1 \times 10^{14} \text{ cm}^{-3}$.

2. Model Spectra

The density sensitivity of the X-ray lines of Fe XXII have been discussed previously by Doschek, Meekins, & Cowan (1973), Mason & Storey (1980), Doschek, Feldman, & Cowan (1981), Phillips et al. (1982), Fawcett et al. (1987), Phillips et al. (1996), and Wargelin et al. (1998) in studies of the X-ray spectra of solar and laboratory high-temperature plasmas. These diagnostics have not received more attention because of the relative weakness of Fe XXII emission lines (the Fe XXII ionization fraction peaks at just 22% and is greater than 1% over the relatively narrow temperature range $T_e \approx 7\text{--}26$ MK; Mazzotta et al. 1998), the relative weakness of $n \rightarrow 2$ lines for $n \geq 4$, and the fact that the critical densities of these transitions are of order 10^{14} cm^{-3} , larger than the densities typically observed in the Sun, tokamaks, and electron beam ion traps. We became interested in the density sensitivity of the $3 \rightarrow 2$ lines of Fe XXII because the critical density of this transition is comparable to the lower limit of the electron density derived from the Fe XVII $I(17.10 \text{ \AA})/I(17.05 \text{ \AA})$ line ratio in the *Chandra* HETG spectrum of EX Hya, and because the

Fe XXII $3 \rightarrow 2$ $I(11.92 \text{ \AA})/I(11.77 \text{ \AA})$ line ratio is anomalous (the 11.92 \AA line is unusually strong) in the *Chandra* HETG spectrum of EX Hya compared to that of the bright late-type binaries HR 1099, Capella, and σ^2 CrB (Ayres et al. 2001, Phillips et al. 2001, and Osten et al. 2003, respectively).

Before wading into the details, we refer the reader to Figure 1, which illustrates the origin of the density dependence of the Fe XXII spectrum. At low densities ($n_e \lesssim 10^{12} \text{ cm}^{-3}$), the Fe XXII electron population is primarily in the $2s^2 2p_{1/2}$ ground state, and collisional excitations are predominantly from the ground state into the $2s^2 2p^2$ manifold (8 levels total) and the $2s^2 3d_{3/2}$ level, both of which decay primarily to ground, producing lines in the extreme ultraviolet (EUV) ($\lambda\lambda = 101\text{--}217 \text{ \AA}$) and at 11.77 \AA , respectively. However, these levels also decay to the $2s^2 2p_{3/2}$ first-excited level with approximately 15% probability, producing lines in the EUV ($\lambda\lambda = 114\text{--}349 \text{ \AA}$) and at 11.93 \AA ; when *that* level decays to ground, it produces a line in the ultraviolet (UV) ($\lambda = 846 \text{ \AA}$). As the density increases ($n_e \gtrsim 10^{13} \text{ cm}^{-3}$), electron population builds up in the $2s^2 2p_{3/2}$ first-excited level because the M1 transition to ground is slow ($A_{21} = 1.47 \times 10^4 \text{ s}^{-1}$). At high densities, the $2s^2 2p_{3/2}$ first-excited level is fed primarily by radiative decays from the $2s^2 2p^2$ manifold. Collisional excitations out of the first-excited level are primarily into the $2s^2 3d_{5/2}$ level, which decays primarily back to the first-excited level, producing a line at 11.92 \AA . Consequently, the Fe XXII 11.92 \AA line is relatively strong in the X-ray spectra of high-density plasmas.

To calculate quantitative models of the X-ray spectrum of Fe XXII, we employed the Livermore X-ray Spectral Synthesizer (LXSS), a suite of IDL codes that calculates spectral models of highly charged ions based on Hebrew University/Lawrence Livermore Atomic Code (HULLAC) atomic data. HULLAC calculates atomic wavefunctions, level energies, radiative transition rates A_{ji} , and oscillator strengths f_{ij} according to the fully relativistic, multiconfiguration, parametric potential method (Klapisch 1971; Klapisch et al. 1977). Electron impact excitation rate coefficients are computed quasi-relativistically in the distorted wave approximation (Bar-Shalom, Klapisch, & Oreg 1988) assuming a Maxwellian velocity distribution. Our Fe XXII model includes electron impact excitation rate coefficients and radiative transition rates for E1, E2, M1, and M2 decays for levels with principal quantum number $n \leq 5$ and azimuthal quantum number $l \leq 4$ for a total of 228 levels. Using these data, LXSS calculates the level populations for a given temperature and density assuming collisional-radiative equilibrium; the line intensities are then simply the product of the level populations and the radiative decay rates.

In a preliminary report, we (Mauche, Liedahl, & Fournier 2003) used LXSS to calculate the X-ray spectrum of Fe XXII for electron densities $n_e = 10^{11}$ to 10^{17} cm^{-3} and electron temperatures $T_e = 6.3, 12.8,$ and 25.5 MK ($\approx \frac{1}{2}, 1,$ and 2 times the temperature at which the Fe XXII ionization fraction peaks; Mazzotta et al. 1998). At the resolution of the *Chandra* HETG, the $2s^2 3d_{3/2}\text{--}2s^2 2p_{1/2}$ line at 11.77 \AA is blended with the (*very* much weaker) $2s^2 3d_{5/2}\text{--}2s^2 2p_{1/2}$ line at 11.76 \AA , and the $2s^2 3d_{5/2}\text{--}2s^2 2p_{3/2}$ line at 11.92 \AA is blended with the (much weaker) $2s^2 3d_{3/2}\text{--}2s^2 2p_{3/2}$ line at 11.93 \AA , so we report as $I(11.92 \text{ \AA})/I(11.77 \text{ \AA})$ the ratio of the sum of these blends. Figure 3 of Mauche, Liedahl, & Fournier (2003) shows that this line ratio has a critical density $n_c \approx 10^{14} \text{ cm}^{-3}$,

is approximately 0.3 at low densities and 1.4 at high densities, and has only a weak temperature dependence.

2.1. Modifications to LXSS: Collisional Excitation

Motivated by the detailed study of Fournier et al. (2001) of the density-sensitive Fe lines in the EUV spectrum of the high-density Frascati Tokamak Upgrade plasma, for this *Letter* we investigated the effect on the Fe XXII $I(11.92 \text{ \AA})/I(11.77 \text{ \AA})$ line ratio of two modifications to the collisional excitation data used in LXSS. First, we investigated the effect of replacing, for all transitions between and among the $2s^22p$ and $2s2p^2$ levels of Fe XXII, the electron impact excitation rate coefficients computed with HULLAC with those of Zhang & Pradhan (1997), computed with the relativistic R-matrix method. At $T_e = 12.8 \text{ MK}$, the Zhang & Pradhan electron impact excitation rate coefficients are larger than those of HULLAC by 1.95 for the $2s^22p_{1/2}-2s^22p_{3/2}$ transition, 0.92–1.70 (average 1.27) for the eight $2s^22p_{1/2}-2s2p^2$ transitions, 1.05–3.23 (average 1.55) for the eight $2s^22p_{3/2}-2s2p^2$ transitions, and 0.45–8.99 (average 2.20) for transitions between levels within the $2s2p^2$ manifold (but only 1.00–1.02 for the four $2s^22p-2s^23d$ transitions). Despite the significant differences between these excitation rate coefficients, we find that for $T_e = 12.8 \text{ MK}$ the Fe XXII $I(11.92 \text{ \AA})/I(11.77 \text{ \AA})$ line ratio increases by 7% at $n_e = 10^{14} \text{ cm}^{-3}$, but the low- and high-density limits are unaffected. Second, we investigated the effect of adding proton excitations for transitions among the levels of the $2s^22p$ and $2s2p^2$ configurations. This was accomplished by fitting the proton impact excitation rate coefficients of Foster, Keenan, & Reid (1997) to an expression of the form $Q(T_e) = 10^{-12} T_e^{-1/2} \sum_{i=1}^3 A_i \exp(-B_i/T_e)$, where $Q(T_e)$ is the proton impact excitation rate coefficient in units of $\text{cm}^3 \text{ s}^{-1}$, and we have assumed that the proton and electron temperatures are equal. Adding proton excitations to the LXSS population kinetics calculation under the assumption that the proton number density $n_p = 0.85 n_e$ (as is appropriate for a high-temperature plasma with solar abundances), we find that for $T_e = 12.8 \text{ MK}$ the Fe XXII $I(11.92 \text{ \AA})/I(11.77 \text{ \AA})$ line ratio increases by 19% at $n_e = 10^{14} \text{ cm}^{-3}$, and the high-density limit increases by 7% to approximately 1.5.

With both of these modifications to LXSS, we recalculated the X-ray spectrum of Fe XXII for electron densities $n_e = 10^{11}$ to 10^{17} cm^{-3} and electron temperatures $T_e = 6.3, 12.8, \text{ and } 25.5 \text{ MK}$. The upper panel of Figure 2 shows that the model Fe XXII $I(11.92 \text{ \AA})/I(11.77 \text{ \AA})$ line ratio has a critical density $n_c \approx 5 \times 10^{13} \text{ cm}^{-3}$, is approximately 0.3 at low densities and 1.5 at high densities, and has only a very weak temperature dependence.

2.2. Modifications to LXSS: Photoexcitation

To investigate the effects of photoexcitation on the Fe XXII $I(11.92 \text{ \AA})/I(11.77 \text{ \AA})$ line ratio, we added to the LXSS population kinetics calculation the photoexcitation rates $(\pi e^2/m_e c) f_{ij} F_\nu(T)$,

where $F_\nu(T)$ is the spectrum of the photoexcitation radiation field. For simplicity, we assume that $F_\nu(T) = (4\pi/h\nu)B_\nu(T_{\text{bb}})$ (i.e., the radiation field is that of a blackbody of temperature T_{bb}) and the dilution factor of the radiation field is equal to $\frac{1}{2}$ (i.e., the X-ray emitting plasma is in close proximity to the source of the photoexcitation continuum). With these assumptions, we used LXSS to calculate the X-ray spectrum of Fe XXII for an electron temperature $T_e = 12.8$ MK, electron densities $n_e = 10^{11}$ to 10^{17} cm $^{-3}$, and photoexcitation temperatures $T_{\text{bb}} = 20, 40, 60, 80,$ and 100 kK. The lower panel of Figure 2 shows that below $T_{\text{bb}} = 60$ kK the Fe XXII $I(11.92 \text{ \AA})/I(11.77 \text{ \AA})$ line ratio has essentially no photoexcitation dependence, but as the photoexcitation temperature increases the line ratio increases at low electron densities and the critical density shifts to higher densities, while the high-density limit is unaffected. Compared to the Fe XVII $I(17.10 \text{ \AA})/I(17.05 \text{ \AA})$ line ratio, the Fe XXII $I(11.92 \text{ \AA})/I(11.77 \text{ \AA})$ line ratio is insensitive to photoexcitation because the $2s^2 2p_{1/2} - 2s^2 2p_{3/2}$ transition in the UV is not optically allowed ($f_{12} = 3.15 \times 10^{-6}$) and the $2s^2 2p_{1/2} - 2s^2 p^2$ transitions lie at such short wavelengths in the EUV.

3. Observations

The *Chandra* HETG/ACIS-S observation of EX Hya was performed between 2000 May 18 9^h41^m and May 19 2^h54^m UT for a total exposure of 59 ks. Extraction of the grating spectra and calculation of the effective area files was accomplished with the CIAO 2.1 suite of software using the reprocessed data products and new calibration data files (version R4CU5UPD8) for sequence 300041. Various aspects of this spectrum have been discussed by Mauche (2000, 2002) and Mauche, Liedahl, & Fournier (2001); here we discuss only a tiny portion ($\lambda \approx 11.60\text{--}12.05 \text{ \AA}$) of the medium-energy grating (MEG) spectrum as it bears on the relative strengths of the Fe XXII $n = 3 \rightarrow 2$ emission lines. This spectrum is shown in Figure 3, where the ordinate is in units of counts s $^{-1} \text{ \AA}^{-1}$, the wavelength bin width $\Delta\lambda = 0.005 \text{ \AA}$, and we have combined \pm first order counts. This portion of the spectrum contains the 11.77 and 11.92 \AA emission lines of Fe XXII as well as the 11.74 \AA emission line of Fe XXIII.

To determine the flux in these emission lines, we fit the MEG spectrum over the $\lambda = 11.60\text{--}12.05 \text{ \AA}$ wavelength interval with a model consisting of a linear background (to account for the thermal bremsstrahlung continuum obvious in the broadband spectrum) and three Gaussians. Assuming a common Gaussian width, the fitting function $f(\lambda; \vec{a}) = a_1 + a_2(\lambda - \lambda_0) + \sum_{i=0}^2 a_{5+2i} \exp[-(\lambda - a_{4+2i})^2 / 2a_3^2] / \sqrt{2\pi}a_3$. To perform the fit, we separately accounted for \pm first orders and used $\Delta\lambda = 0.005 \text{ \AA}$ bins, so there were 180 data points and 171 degrees of freedom (dof). The resulting fit, combining \pm first orders, is shown by the thick histogram in Figure 3. It gives $\chi^2/\text{dof} = 104/171 = 0.60$ and fit parameters as follows: Gaussian width $a_3 = 1.4_{-0.9}^{+1.6} \text{ m\AA}$ and line wavelengths and fluxes $I(11.740 \text{ \AA}) = 7.74 (\pm 0.80) \times 10^{-5}$, $I(11.776 \text{ \AA}) = 4.27 (\pm 0.67) \times 10^{-5}$, and $I(11.923 \text{ \AA}) = 4.52 (\pm 0.68) \times 10^{-5}$ photons cm $^{-2}$ s $^{-1}$, where the errors on the wavelengths are $\pm 1\text{--}2 \text{ m\AA}$ and all errors are 1σ (68% confidence) for one interesting degree of freedom. Formally (e.g., Bevington 1960), the $I(11.92 \text{ \AA})/I(11.78 \text{ \AA})$ line ratio equals 1.06 ± 0.23 (68% confidence), but this

propagation of errors ignores a subtle interplay between the error bars of the numerator and denominator of this ratio. To generate more rigorous values for the error bars of this ratio, we used a Monte Carlo technique with 10^6 realizations to determine that the observed $I(11.92 \text{ \AA})/I(11.78 \text{ \AA})$ line ratio equals 1.06 and the errors are $^{+0.26}_{-0.20}$ (68% confidence), $^{+0.48}_{-0.32}$ (90% confidence), and $^{+0.89}_{-0.47}$ (99% confidence). This best-fit line ratio and these error envelopes are shown superposed on both panels of Figure 2.

4. Analysis

Figure 2 shows that the combination of our LXSS models and *Chandra* HETG spectrum places significant constraints on the density of the $T_e \approx 12$ MK plasma in EX Hya. Specifically, allowing for a factor-of-two uncertainty in the electron temperature, the upper panel of Figure 2 shows that the electron density $n_e = 1.0^{+2.0}_{-0.5} \times 10^{14} \text{ cm}^{-3}$ at 68% confidence, $n_e \geq 3.2 \times 10^{13} \text{ cm}^{-3}$ at 90% confidence, and $n_e \geq 1.7 \times 10^{13} \text{ cm}^{-3}$ at 99% confidence. Conversely, the lower panel of Figure 2 shows that the electron density can be arbitrarily low if the photoexcitation temperature $T_{\text{bb}} \gtrsim 100$ kK, but that alternative is excluded by UV observations of EX Hya. First, assuming that the distance to EX Hya is 100 pc, that the radius of its white dwarf is $R_{\text{wd}} = 10^9$ cm, that its 1010 \AA flux density equals $2.5 \times 10^{-13} \text{ erg cm}^{-2} \text{ s}^{-1} \text{ \AA}^{-1}$ (Mauche 1999), and that 100% of this emission is due to a 100 kK hotspot (i.e., assuming that the white dwarf, accretion disk, and accretion curtains do not radiate in the UV), the fractional emitting area of the spot is approximately 0.5%, far smaller than is inferred from optical and UV light curves of mCVs. Second, fits to EX Hya’s UV spectrum yield effective temperatures $T_{\text{eff}} \approx 25$ kK (Greeley et al. 1997; Eisenbart et al. 2002), far lower than that required to produce the anomalous Fe XXII $I(11.92 \text{ \AA})/I(11.77 \text{ \AA})$ line ratio via photoexcitation.

5. Discussion

To date, four different spectroscopic diagnostics have provided evidence of high densities in the X-ray-emitting plasma of the intermediate polar EX Hya. Hurwitz et al. (1997) used the line ratio of the Fe XX/Fe XXIII 133 \AA blend to the Fe XXI 129 \AA line observed in the 1994 *Extreme Ultraviolet Explorer* spectrum of EX Hya to infer $n_e \gtrsim 10^{13} \text{ cm}^{-3}$ under the assumption that the plasma temperature $T_e = 10$ MK. Using the *Chandra* HETG spectrum of EX Hya, Mauche (2002) showed that the He-like ion R line ratios of O, Ne, Mg, Si, and S are all in their high-density limit; Mauche, Liedahl, & Fournier (2001) used the Fe XVII $I(17.10 \text{ \AA})/I(17.05 \text{ \AA})$ line ratio to infer $n_e \gtrsim 2 \times 10^{14} \text{ cm}^{-3}$ for its $T_e \approx 4$ MK plasma; and we here used the Fe XXII $I(11.92 \text{ \AA})/I(11.77 \text{ \AA})$ line ratio to infer $n_e \approx 1 \times 10^{14} \text{ cm}^{-3}$ for its $T_e \approx 12$ MK plasma. Of these diagnostics, the Fe XXII line ratio is the most reliable because it has the highest critical density and is the least sensitive to temperature and photoexcitation. We conclude first that the *Chandra* HETG spectrum of EX Hya requires plasma densities that are orders of magnitude greater than those typically observed in the Sun or other late-type stars, and second that the Fe XXII

$I(11.92 \text{ \AA})/I(11.77 \text{ \AA})$ line ratio [like the Fe XVII $I(17.10 \text{ \AA})/I(17.05 \text{ \AA})$ line ratio] is a useful density diagnostic for sources like mCVs in which the plasma densities are high and the efficacy of the He-like ion density diagnostic is compromised by the presence of a bright UV continuum. Finally, we note that our density determinations for EX Hya are consistent with those expected for plasma in the accretion column, where $n_e \propto T_e^{-1}$. Additional density diagnostics are needed to begin to map the temperature/density profile of the accretion column of this and other mCVs.

We thank H. Tananbaum for the generous grant of Director's Discretionary Time that made possible the *Chandra* observations of EX Hya. Support for this work was provided in part by NASA through *Chandra* Award Number DD0-1004B issued by the *Chandra* X-Ray Observatory Center, which is operated by the Smithsonian Astrophysical Observatory for and on behalf of NASA under contract NAS8-39073. This work was performed under the auspices of the U.S. Department of Energy by University of California Lawrence Livermore National Laboratory under contract No. W-7405-Eng-48.

REFERENCES

- Ayres, T. R., et al. 2001, *ApJ*, 549, 554
- Bar-Shalom, A., Klapisch, M., & Oreg, J. 1988, *Phys. Rev. A*, 38, 1773
- Bevington, P. R. 1969, *Data Reduction and Error Analysis for the Physical Sciences* (New York: McGraw-Hill)
- Blumenthal, G. R., Drake, G. W. F., & Tucker, W. H. 1972, *ApJ*, 172, 205
- Doschek, G. A., Feldman, U., & Cowan, R. D. 1981, *ApJ*, 245, 315
- Doschek, G. A., Meekins, J. F., & Cowan, R. D. 1973, *Sol. Phys.*, 29, 125
- Eisenbart, S., Beuermann, K., Reinsch, K., & Gänsicke, B. T. 2002, *A&A*, 382, 984
- Fawcett, B. C., Jordan, C., Lemen, J. R., & Phillips, K. J. H. 1987, *MNRAS*, 225, 1013
- Foster, V. J., Keenan, F. P., & Reid, R. H. G. 1997, *At. Data Nucl. Data Tables*, 67, 99
- Fournier, K. B., et al. 2001, *ApJ*, 561, 1144
- Frank, J., King, A., & Raine, D. 1992, *Accretion Power in Astrophysics* (Cambridge: CUP)
- Gabriel, A. H., & Jordan, C. 1969, *MNRAS*, 145, 241
- Greeley, B. W., Blair, W. P., Long, K. S., & Knigge, C. 1997, *ApJ*, 488, 419
- Hurwitz, M., Sirk, M., Bowyer, S., & Ko, Y.-K. 1997, *ApJ*, 477, 390

- Klapisch, M. 1971, *Computer Phys. Comm.*, 2, 239
- Klapisch, M., Schwob, J., Fraenkel, B., & Oreg, J. 1977, *J. Opt. Soc. Am.*, 67, 148
- Mason, H. E., & Storey, P. J. 1980, *MNRAS*, 191, 631
- Mauche, C. W. 1999, *ApJ*, 520, 822.
- Mauche, C. W. 2000, *BAAS*, 32, 1561
- Mauche, C. W. 2002, in *The Physics of Cataclysmic Variables and Related Objects*, ed. B. T. Gänsicke, K. Beuermann, & K. Reinsch (San Francisco: ASP), 113
- Mauche, C. W., Liedahl, D. A., & Fournier, K. B. 2001, *ApJ*, 560, 992
- Mauche, C. W., Liedahl, D. A., & Fournier, K. B. 2003, in *IAU Colloquium No. 190—Magnetic Cataclysmic Variables*, ed. M. Cropper & S. Vriellmann (San Francisco: ASP), in press (astro-ph/0301633)
- Mazzotta, P., Mazzitelli, G., Colafrancesco, S., & Vittorio, N. 1998, *A&AS*, 133, 403
- Osten, R. A., Ayres, T. R., Brown, A., Linsky, J. L., & Krishnamurthi, A. 2003, *ApJ*, 582, 1073
- Phillips, K. J. H., Bhatia, A. K., Mason, H. E., & Zarro, D. M. 1996, *ApJ*, 466, 549
- Phillips, K. J. H., et al. 1982, *ApJ*, 256, 774
- Phillips, K. J. H., Mathioudakis, M., Huenemoerder, D. P., Williams, D. R., Phillips, M. E., & Keenan, F. P. 2001, *MNRAS*, 325, 1500
- Porquet, D., Mewe, R., Dubau, J., Raassen, A. J. J., & Kaastra, J. S. 2001, *A&A*, 376, 1113
- Wargelin, B. J., Beiersdorfer, P., Liedahl, D. A., Kahn, S. M., & von Goeler, S. 1998, *ApJ*, 496, 1031
- Zhang, H. L., & Pradhan, A. K., 1997, *A&AS*, 123, 575

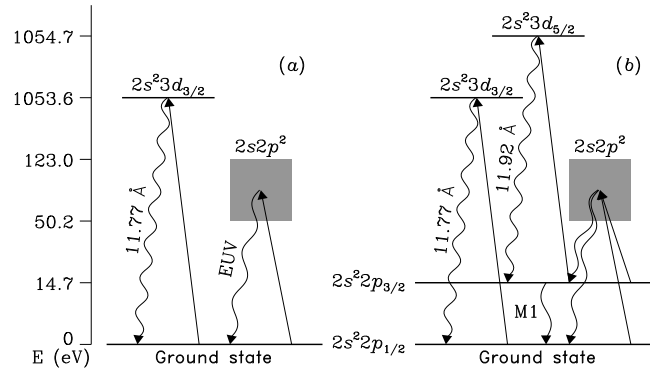


Fig. 1.— Schematic diagram of the dominant collisional and radiative processes of Fe XXII for electron densities $n_e = 10^{11}$ (a) and 10^{17} cm^{-3} (b). Collisional excitations are indicated by upward-pointing straight lines; radiative decays are indicated by downward-pointing wavy lines and are labeled with the wavelength of the transition in Angstroms.

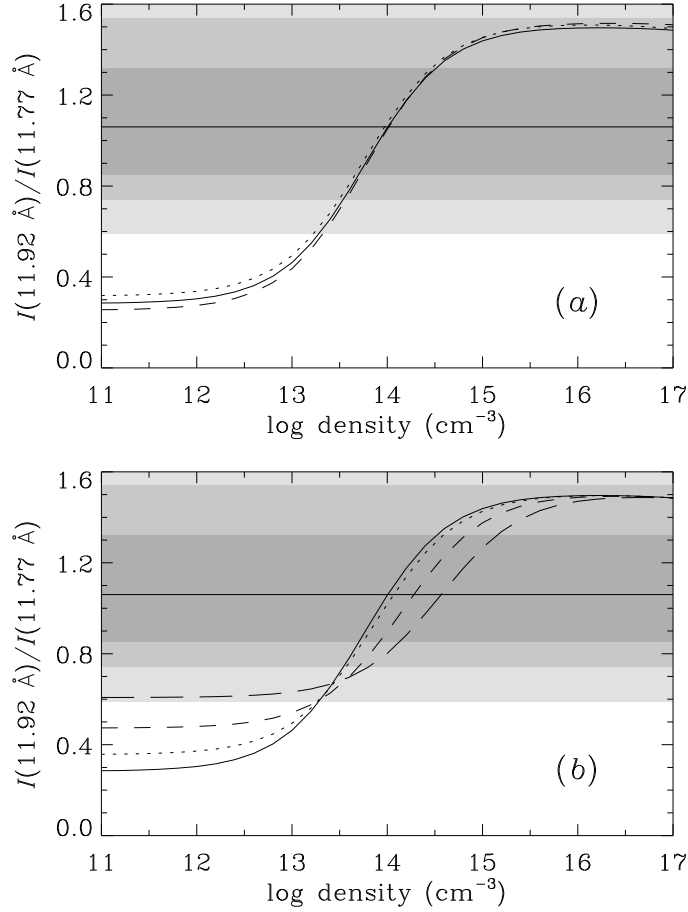


Fig. 2.— LXSS model Fe XXII $I(11.92 \text{ \AA})/I(11.77 \text{ \AA})$ line ratio as a function of electron density for (a) electron temperatures $T_e = 6.3, 12.8,$ and 25.5 MK (*dotted, solid, and dashed curves, respectively*) and (b) electron temperature $T_e = 12.8$ MK and photoexcitation temperatures $T_{bb} = 0, 60, 80,$ and 100 kK (*solid, dotted, short dashed, and long dashed curves, respectively*). Horizontal line and the dark, medium, and light shaded stripes indicate respectively the value and 68%, 90%, and 99% confidence error envelopes of the line ratio measured in EX Hya.

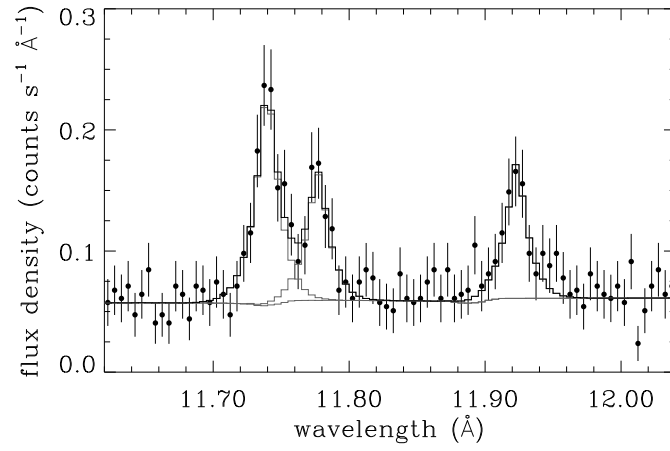


Fig. 3.— Detail of the *Chandra* MEG spectrum of EX Hya in the neighborhood of the Fe XXII $3 \rightarrow 2$ lines. Data are shown by the filled circles with error bars and the net and separate contributions to the model fit are shown by the histograms. Data combines \pm first orders and are binned to 0.005 Å.